Design of steam condensation temperature for an innovative solar thermal power generation system using cascade Rankine cycle and two-stage accumulators

Guangtao Gao[a], Jing Li[b,*], Pengcheng Li[c], Jingyu Cao[a], Gang Pei[a, †], Yousef N. Dabwan[a], Yuehong Su[b]

[a]*Department of Thermal Science and Energy Engineering, University of Science and Technology of China, 96 Jinzhai Road, Hefei, 230026, China*

[b]*Department of Architecture and Built Environment, University of Nottingham, University Park, Nottingham, NG7 2RD, UK*

[c]*School of Automobile and Traffic Engineering, Hefei University of Technology, 193 Tunxi Road, Hefei, 230009, China*

* Corresponding author. Tel.: +86-551-6360-7517; fax: +86-551-6360-7517.

E-mail address: lijing83@ustc.edu.cn

† Corresponding author. Tel.: +86-551-6360-7367; fax: +86-551-6360-7367.

E-mail address: peigang@ustc.edu.cn

Abstract: An innovative solar thermal power generation system using cascade steam-organic Rankine cycle (SORC) and two-stage accumulators has recently been proposed. This system offers a significantly higher heat storage capacity than conventional direct steam generation (DSG) solar power plants. The steam condensation temperature (T_2) in the proposed system is a crucial parameter because it affects the SORC efficiency (η_{SORC}) in normal operations and the power conversion of the bottoming organic Rankine cycle (ORC) in the unique heat discharge process. The present study develops a methodology for the design of T_2 with respect to a new indicator, that is, the equivalent heat-to-power efficiency (η_{eq}). η_{eq} is a compromise between the efficiencies in different operation modes. The effects of main steam temperature (T_1), Baumann factor (a), mass of storage water (M_w), and ORC working fluid on T_2 are investigated. Results show that η_{eq} is a better indicator than η_{SORC}. The optimum steam condensation temperature ($T_{2,opt}$) that corresponds to the maximum η_{eq} ($\eta_{eq,max}$) is generally higher than that based on the maximum η_{SORC}. $T_{2,opt}$ reduces as T_1, a, and M_w decrease. $\eta_{eq,max}$ rises with the increment of T_1 and the decrement of a and M_w. Pentane is a more preferable ORC fluid than benzene and R245fa. The $T_{2,opt}$ and $\eta_{eq,max}$ of pentane are, respectively, 139-190 °C and 20.93%-24.24%, provided that T_1 ranges between 250 °C and 270 °C, a varies from 0.5 to 1.5, and M_w changes from 500 ton to 1500 ton.

Keywords: steam condensation temperature; direct steam generation; cascade Rankine cycle; two-stage accumulators; wet steam turbine.

Nomenclature

A	aperture area, m^2	SRC	steam Rankine cycle
a	Baumann factor	TV	throttle valve
C	coefficient	V	valve
h	enthalpy, kJ/kg	*Subscripts*	
I	solar irradiance, W/m^2	*0…8*	number
L	receiver length, m	*a*	ambient
M	mass, ton	*av*	average
$\dot{m}$	mass flow rate, kg/s	*col*	solar collector
q	heat loss, W/m	*DN*	direct normal
$\dot{q}$	absorbed heat power, kW	*eq*	equivalent
T	temperature, °C	*g*	generator
t	operating time, hour	*in*	inlet
v	speed, m/s	*l*	liquid
$\dot{w}$	work, kW	*loss*	heat loss
y	steam wetness, %	*max*	maximum
γ	absorbed heat power ratio	*min*	minimum
ε	isentropic efficiency, %	*opt*	optical/optimum
η	thermal efficiency, %	*out*	outlet
τ	operating time ratio	*OT*	ORC dry turbine
Abbreviations		*pinch*	pinch point
DSG	direct steam generation	*s*	isentropic
HTA	high-temperature accumulator	*sh*	superheated
LTA	low-temperature accumulator	*ST*	wet steam turbine
ORC	organic Rankine cycle	*total*	total
P	pump	*v*	vapor
SORC	steam-organic Rankine cycle	*w*	water/wind

1. Introduction

Direct steam generation (DSG) technology is burgeoning in the field of solar thermal power systems. As water is directly heated in solar collectors, the oil-water or molten salt-water heat exchangers are unnecessary. Expensive oil or molten salt can be replaced with cheap water. The levelized electricity cost of solar thermal power plants is reduced by DSG technology [1-4]. Commercial DSG plants generally use single-stage steam accumulators for heat storage and wet steam turbines for power conversion [5-8]. The saturated steam generated from solar collectors or accumulators is directly injected into the wet steam turbine. An example is the Planta Solar 10 plant, the system schematic diagram of which is shown in Fig. 1 [5]. Nevertheless, some technical challenges for conventional DSG systems remain. First, the wet steam turbine suffers from inefficiency due to the presence of moisture in the expansion process [9-10]. Generally, exhaust steam wetness should not be higher than 14% [11-12]. Second, flashing steam pressure and mass flow rate decrease during the heat discharge process, thereby resulting in off-design operations and complex system control strategies [13-14]. Third, the acceptable temperature drop of water in accumulators is small to avoid inefficient power generation, hence leading to a limited storage capacity [15-16].

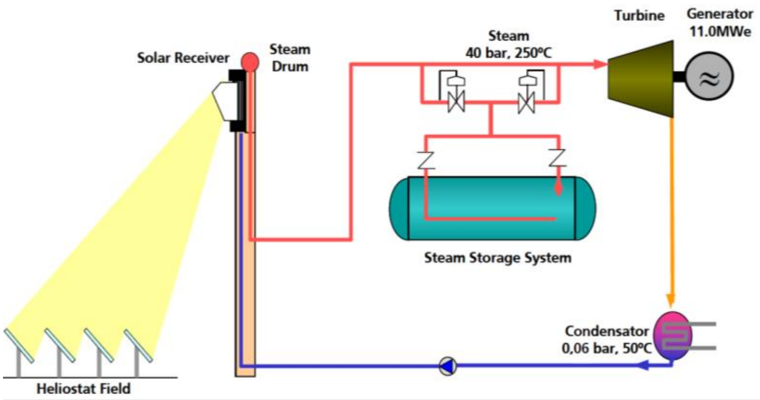

Fig.1 Schematic diagram of the Planta Solar 10 plant [5].

The above problems can be solved or alleviated by an innovative DSG system that uses a cascade steam-organic Rankine cycle (SORC) and two-stage accumulators (Fig. 2) [17]. In normal working conditions, water in the low-temperature accumulator (LTA) is heated and partially vaporized by solar collectors. The saturated steam is used to drive the SORC, and the hot water is stored in the high-temperature accumulator (HTA). Two steps are used for the heat discharge. In the first step, heat discharge occurs in the HTA, which is similar to that in conventional DSG plants. The energy is used to drive the SORC. The second step contributes greatly to the increased storage capacity. In this step, the stored hot water moves from the HTA into the LTA through an intermediate heat exchanger, and the released heat is used only to drive the bottoming organic Rankine cycle (ORC). The system has considerable potential in easing the challenges associated with wet steam turbines. First, exhaust steam wetness can be reduced by elevating ORC evaporation temperature. Second, the low-pressure cylinders in wet steam turbines can be omitted by introducing an ORC. Unlike water, dry organic fluid will enter a superheat state if it expands from a saturated vapor state, thereby offering a safe and efficient expansion process [18]. The ORC turbine is typically a dry turbine with an isentropic efficiency of up to 90% [19]. Third, because water is a heat transfer medium rather than a working fluid in the second step of the heat discharge process, the temperature drop of hot water can increase remarkably. Meanwhile, the bottoming ORC can work in design conditions by adjusting the hot water mass flow rate. Overall, the proposed system using a cascade Rankine cycle and two-stage accumulators is promising.

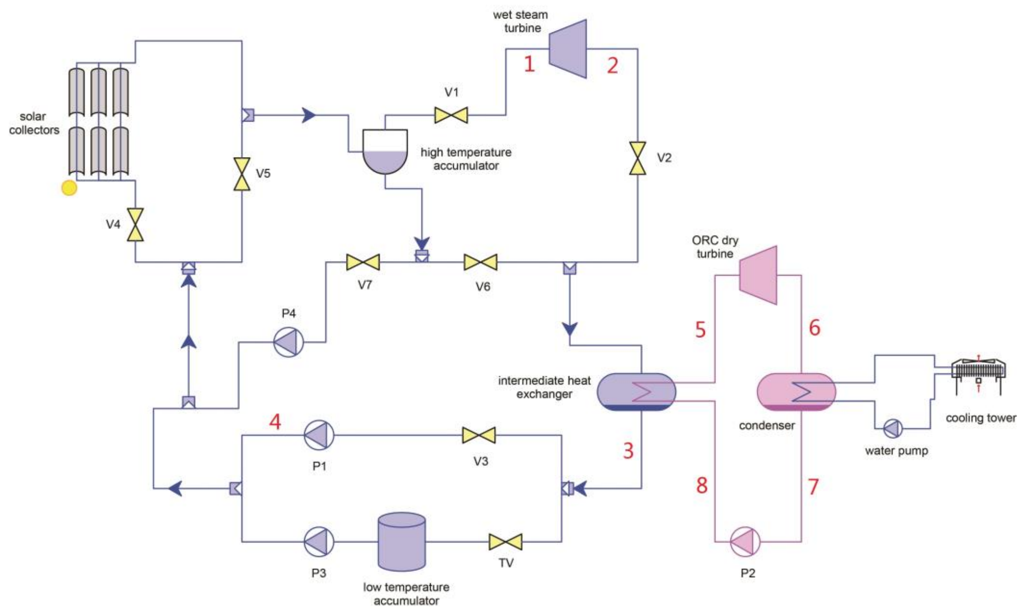

Fig.2 Schematic diagram of the DSG-SORC system using two-stage accumulators.

Notably, the steam condensation temperature of the topping steam Rankine cycle

(SRC) in the proposed system (i.e., T_2) is a crucial parameter because of the following reasons.

(1) The heat discharge process is unique. Compared with conventional DSG systems, the DSG-SORC system has an LTA. In the second step of the heat discharge process, water flows from the HTA to the LTA through a heat exchanger, and the heat is used only to drive the bottoming ORC. On the one hand, the storage capacity and power production of the system are significantly elevated by this process due to the large temperature drop of water. On the other hand, the ORC has a lower heat-to-power efficiency than the SORC. A high ORC evaporation temperature (i.e., a high T_2) is preferred for the sake of efficient power conversion in the heat discharge process. Under such conditions, the payback time of the additional solar collectors used to increase the heat storage capacity is shortened.

(2) In normal working conditions, steam is generated directly in the solar field and is used to drive the SORC. T_2 that leads to the highest power efficiency in the heat discharge process is unlikely to offer a maximum SORC efficiency. T_2 in design shall be determined by the thermodynamic performance in different operation modes.

(3) T_2 affects exhaust steam wetness. Exhaust steam wetness increases with the decrement of T_2 [20], thereby resulting in a low expansion efficiency and high technical requirement for turbomachinery.

(4) T_2 may affect the heat storage capacity at given accumulator size and HTA operating temperature. The heat transfer between water and organic fluids in the heat discharge process is related to T_2. The temperature of water after discharge may vary at different T_2.

To date, some studies have been conducted to optimize the intermediate parameters in a cascade cycle, mainly focusing on the SORC and dual-loop ORC. For SORC systems, Li et al. studied a single-stage accumulator-based DSG-SORC system and found there is an ORC evaporation temperature at which the system thermal efficiency is theoretically maximized [21-22]. Liu et al. found that for each cold source temperature, an optimum steam turbine exhaust pressure is available [23]. Ziółkowski et al. pointed out that the specific volume of exhaust steam is reduced by increasing steam condensation temperature, thereby resulting in the reduced size of low-pressure cylinders [24]. Choi et al. concluded that for a trilateral cycle-based SORC system, the amount of heat recovered from the evaporator and the amount of heat transmitted to the lower cycle are reduced together, according to an increase in the boundary temperature [25]. Furthermore, Nazari et al. found that the steam condenser and organic vapor generator present major exergy destruction [26]. For dual-loop ORC systems, Shu et al. concluded that a low condensation temperature in the high-temperature loop is beneficial to performance optimization [27-29]. Yang et al. found that the optimal condensation temperature of the high-temperature cycle and the evaporation temperature of the low-temperature cycle are kept nearly constant under various operating conditions of a CNG engine [30]. Song et al. found that the pinch point of the low-temperature loop is associated with the condensation temperature of the high-temperature loop [31-32]. Furthermore, Zhou et al. found that the variation trend of the net power output in the low-temperature loop is related to the pinch point position in a zeotropic mixture-characterized system. [33] Ge et al. indicated that net power output decreases as the condensation dew point temperature in the high-temperature loop increases [34]. Habibi et al. studied a solar-driven ammonia-water regenerative Rankine cycle and concluded that the thermo-economic performance of the system improves by decreasing the ammonia-water condensation temperature [35]. Sadreddini et al. found that a higher turbine inlet temperature, higher turbine inlet pressure, and lower condenser pressure lead to a high exergy efficiency in a transcritical CO_2 cycle-based cascade ORC system [36]. Cao et al. discovered that for a gas turbine and cascade CO_2 combined cycle, the design parameters of supercritical CO_2 compressor inlet pressure and inlet temperature exert a non-monotonous effect on the cascade CO_2 net power [37]. Particularly, Yuan et al. inferred that the optimum intermediate ORC condensation pressure is variable on the basis of different evaluation indexes [38]. Other cascade systems combined with refrigeration cycles have also been studied. For example, Xia et al. analyzed a cascade system comprising a CO_2 Brayton cycle, an ORC, and an ejector refrigeration cycle. The results showed that the increase of ORC turbine inlet pressure is beneficial to thermodynamic and exergoeconimic performances [39]. Wu et al. studied a cascade system combined with supercritical CO_2 recompression Brayton/absorption refrigeration cycle and found that the heat-end and cold-end temperature difference in the generator affect the energy utilization factor and exergy efficiency [40].

Notably, the above systems only have a sole heat-to-power conversion mode. The topping and bottoming cycles work simultaneously, and heat is converted into power by the cascade cycle. A main objective of optimization is to maximize cascade cycle efficiency. In contrast to those systems, the proposed DSG-SORC system only uses the bottoming cycle to generate power in the second step of the heat discharge process. The annual yield is not solely contributed by the cascade operation mode, and the conventional design criteria may not be applicable.

The current study develops a methodology to design the steam condensation temperature for the proposed system. A new indicator, namely, the equivalent heat-to-power efficiency, is established. The indicator considers the cascade SORC efficiency and bottoming ORC efficiency. The effects of main steam temperature, Baumann factor, mass of storage water, and ORC working fluid on the optimum steam condensation temperature are investigated. The potential of the DSG-SORC system is further explored with the design.

2. System description

Figure 2 presents the schematic diagram of the DSG-SORC system using two-stage accumulators. The system is composed of SRC, ORC, and accumulators (i.e., HTA and LTA). The SRC contains solar collectors, the wet steam turbine, and water pumps. The ORC includes the ORC dry turbine, condenser, cooling tower, and pumps. The intermediate heat exchanger acts as a condenser in the SRC and as an evaporator in the ORC. The system can operate in three modes: simultaneous heat collection and power conversion mode, first-step heat discharge mode, and second-step heat discharge mode. The details are as follows.

(1) Simultaneous heat collection and power conversion mode. The system works in this normal case when solar radiation is available. The power is produced via the SORC. V1, V2, V3, and V4 are open. P1, P2, and P3 are run. V7 is open, and P4 works when the dryness fraction at the solar collectors' outlet needs to be controlled. The unmentioned valves and pumps are closed or off-work. Water in the LTA is heated and partially vaporized through the solar collectors. The hot water is stored in the HTA. The saturated steam is expanded through the wet steam turbine to generate electrical power. Thereafter, the exhaust steam is condensed into water via the intermediate heat exchanger and is pressurized by P1 before being sent back to the solar collectors. The condensation heat is used to evaporate the ORC working fluid to saturated vapor, which is expanded through the ORC dry turbine to produce electrical power. Then, the exhaust organic vapor is condensed into liquid through the condenser and is sent back to the intermediate heat exchanger by P2. Depending on the solar radiation, the flow rate through P3 can be altered to guarantee a constant temperature in the HTA and a steady power conversion of the SORC.

(2) First-step heat discharge mode. V1, V2, V3, and V5 are open. P1 and P2 are run. The hot water in the HTA is partially vaporized by depressurization and is used to drive the SORC. The exhaust steam is condensed and pumped back to the HTA. The temperature drop of the HTA is limited as the wet steam and organic fluid turbines would suffer from an inefficient off-design operation [13-14]. The LTA is not involved in this step.

(3) Second-step heat discharge mode. V6 and throttle valve (TV) are open, and P2 is run. The dissipated hot water in the HTA flows into the LTA via the intermediate heat exchanger, and the released heat is used only to drive the bottoming ORC. This step can generate much more electricity than the first step due to the remarkable drop in water temperature.

3. Mathematical models

For the proposed system, subcritical cycles are considered for the SRC and ORC.

When benzene using as ORC fluid, for example, the thermodynamic processes expressed in the T-s diagram are shown in Fig. 3. The blue and red lines represent the SRC and ORC, respectively. The numbers indicate the thermodynamic states of water and organic fluid that corresponds to the marks in Fig. 2. Furthermore, the thermal and friction losses in the pipes and heat exchangers are neglected. The kinetic and potential energy changes are disregarded in the simulation.

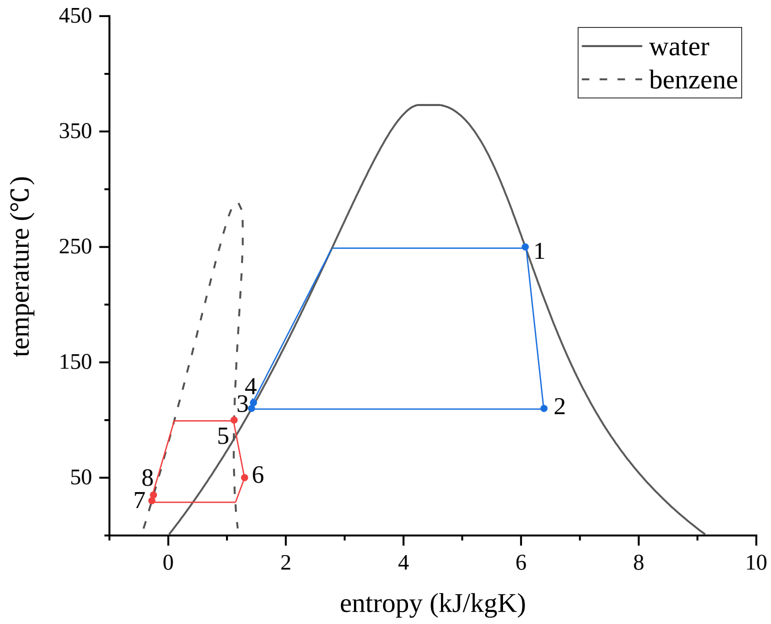

Fig.3 T-s diagram of the DSG-SORC system using two-stage accumulators.

A wet steam turbine is adopted for the topping SRC. This type of turbine has been used for decades, especially in nuclear power plants [20]. After long-term development, modern turbines are now able to handle binary-phase steam at dryness lower than 90%. One advantage of steam turbines is their high power capacity, which can be two orders of magnitude higher than that of positive displacement expanders. This advantage results in a low cost proportion of the power block in the whole solar plant and short payback period.

In the study, the first-step heat discharge is omitted for the following reasons.

(1) The process is similar to that in conventional DSG solar plants and is not essential in the proposed system. The first-step heat discharge is accompanied by the off-design operation of the turbine and has a relatively small power capacity, which is attributed to either a short discharge time or an inefficient power conversion. For

example, the Planta Solar 10 plant has a saturated water heat storage capacity of 50 min operation at 50% turbine workload [5]. In the Khi Solar One plant, 10.5 h of discharging time are needed to produce power equivalent to that generated in 3 h nominal operation [16].

(2) The first-step heat discharge may be less efficient than the second-step heat discharge. As shown in the following sections, the optimized ORC efficiency can be equal to approximately 70% of the SORC's. Compared with the first-step heat discharge that suffers from part-load operation, the second-step heat discharge enables stable power conversion and is possibly more efficient.

(3) The process leads to a large stress range for the materials. The pressure in the HTA decreases as the first-step heat discharge proceeds, whereas it is almost constant in the second-step heat discharge. During the periodical charge and discharge, the stress of the material e.g., stainless steel, fluctuates. A large stress range shortens the life span of the pressure vessel.

3.1 Solar collectors

Common solar collectors in DSG applications include parabolic trough collectors (PTCs), linear Fresnel collectors, and heliostats. However, only mature and predominant PTCs are exemplified in the following analysis. The system advisor model (SAM) software created by National Renewable Energy Laboratory (NREL) is adapted to simulate the heat collection in the PTCs [41]. The overall efficiency of the solar collector (η_{col}) is defined as the optical efficiency (η_{opt}) minus an efficiency penalty term (η_{loss}) representing the receiver's heat loss [42-43].

$$\eta_{col} = \eta_{opt} - \eta_{loss} = \eta_{opt} - \frac{Lq_{loss,av}}{A_{col}I_{DN}} \tag{1}$$

where L is the receiver length (m), $q_{loss,av}$ is the receiver's average heat loss (W/m), A_{col} is the aperture area of the solar collector (m^2), and I_{DN} is the direct normal solar irradiance (W/m^2).

In an entire loop of the solar field, $q_{loss,av}$ is calculated by [44-45]

$$q_{loss,av} = C_0 + C_5\sqrt{v_w} + \left(C_1 + C_6\sqrt{v_w}\right)\frac{T_{in} + T_{out} - T_a}{2} +$$

$$(C_2 + C_4 I_{DN}) \frac{T_{in}^2 + T_{in} T_{out} + T_{out}^2}{3} + C_3 \frac{(T_{in}^2 + T_{out}^2)(T_{in} + T_{out})}{4} \quad (2)$$

where $C_0 \ldots C_6$ are the heat loss coefficients; v_w is the wind speed (m/s); T_{in} and T_{out} are the working fluid inlet and outlet temperatures, respectively (°C), and T_a is the ambient temperature (°C). Equation (2) correlates the heat loss with the working fluid temperature (C_2 and C_3), the heating of the receiver above the working fluid temperature by the sun (C_4), and the effects of the ambient temperature and wind speed (C_1, C_5, and C_6).

The specific parameters of the PTCs for heat collection in SAM, as well as their default values, are listed in Table 1 [41]. L, A_{col}, and η_{opt} are the intrinsic properties of the Euro Trough ET150 collector. Heat loss coefficients are determined by fitting the test curves for Schott's 2008 PTR70 receiver. The details can be found in NREL's technical report [45].

Table 1 Specific parameters of PTCs in SAM [41].

Terms	**PTCs**
Receiver length, L	150 m
Aperture area, A_{col}	817.5 m^2
Optical efficiency, η_{opt}	76.77%
Heat loss coefficient, C_0	4.05
Heat loss coefficient, C_1	0.247
Heat loss coefficient, C_2	-0.00146
Heat loss coefficient, C_3	5.65e-06
Heat loss coefficient, C_4	7.62e-08
Heat loss coefficient, C_5	-1.7
Heat loss coefficient, C_6	0.0125

3.2 Turbines

The work generated by the wet steam turbine is determined by

$$\dot{w}_{ST} = \dot{m}_{SRC}(h_1 - h_2) = \dot{m}_{SRC}(h_1 - h_{2s})\varepsilon_{ST} \quad (3)$$

where ε_{ST} is the isentropic efficiency of the wet steam turbine. It is associated with steam wetness, as described by the Baumann rule, which is a longstanding empirical rule in the history of turbomachinery [9,20].

$$\varepsilon_{ST} = \varepsilon_{ST,sh}(1 - a y_{av}) \tag{4}$$

$$y_{av} = (y_1 + y_2)/2 \tag{5}$$

where $\varepsilon_{ST,sh}$ is the reference isentropic efficiency assuming that the turbine works with superheated steam; *a* is an empirical coefficient known as the Baumann factor, that is usually assumed to be 1.0, although various experiments carried out on wet steam turbines provide a range of values for a, varying from 0.4 to 2.0 [46]; and y_1 and y_2 are the main steam and exhaust steam wetness, respectively.

For given main steam and steam condensation temperature, h_1, h_{2s}, and y_1 are determined. y_2 can be derived by combining Eqs. (4) and (5) and the definition of turbine isentropic efficiency.

$$\varepsilon_{ST} = \frac{h_1 - h_2}{h_1 - h_{2s}} = \frac{h_1 - (y_2 h_{2,l} + (1 - y_2) h_{2,v})}{h_1 - h_{2s}} \tag{6}$$

The result is

$$y_2 = \frac{\varepsilon_{ST,sh}(2 - a y_1)(h_1 - h_{2s}) - 2(h_1 - h_{2,v})}{\varepsilon_{ST,sh} a (h_1 - h_{2s}) - 2(h_{2,l} - h_{2,v})} \tag{7}$$

where $h_{2,l}$ and $h_{2,v}$ are respectively the saturated water and steam enthalpies at steam condensation temperature.

The work generated by the ORC dry turbine is calculated by

$$\dot{w}_{OT} = \dot{m}_{ORC}(h_5 - h_6) = \dot{m}_{ORC}(h_5 - h_{6s})\varepsilon_{OT} \tag{8}$$

where ε_{OT} is the isentropic efficiency of the ORC dry turbine. Unlike ε_{ST}, ε_{OT} can be considered as a constant because the ORC dry turbine is operated without liquid droplets.

3.3 Intermediate heat exchanger

In normal working conditions, the heat balance in the intermediate heat exchanger is expressed by

$$\dot{m}_{SRC}(h_2 - h_3) = \dot{m}_{ORC}(h_5 - h_8) \tag{9}$$

In the second step of the heat discharge process, if the minimum temperature difference (ΔT_{min}) occurs in pinch point, then the heat balance is determined by

$$\dot{m}_w(h_{1,l} - h_{w,pinch}) = \dot{m}_{ORC}(h_{5,v} - h_{5,l}) \quad (10)$$

If ΔT_{min} takes place in water outlet, then the heat balance is calculated by

$$\dot{m}_w(h_{1,l} - h_{w,out}) = \dot{m}_{ORC}(h_5 - h_8) \quad (11)$$

where $\dot{m}_w$ is the hot water mass flow rate; $h_{1,l}$ is the saturated water enthalpy at main steam temperature; $h_{w,pinch}$ is the water enthalpy at the temperature of $T_5 + \Delta T_{min}$; $h_{5,l}$ and $h_{5,v}$ are respectively the saturated organic liquid and vapor enthalpies at the inlet temperature of the ORC dry turbine (T_5); and $h_{w,out}$ is the outlet water enthalpy at the temperature of $T_8 + \Delta T_{min}$.

3.4 Pumps

The works required by the SRC water pump and ORC pump are respectively calculated by

$$\dot{w}_{P,SRC} = \dot{m}_{SRC}(h_4 - h_3) = \dot{m}_{SRC}(h_{4s} - h_3)/\varepsilon_P \quad (12)$$

$$\dot{w}_{P,ORC} = \dot{m}_{ORC}(h_8 - h_7) = \dot{m}_{ORC}(h_{8s} - h_7)/\varepsilon_P \quad (13)$$

where ε_P is the pump isentropic efficiency.

3.5 Normal SORC efficiency

The topping SRC thermal efficiency is expressed by

$$\eta_{SRC} = \frac{\dot{w}_{SRC}}{\dot{q}_{SRC}} = \frac{\dot{w}_{ST}\varepsilon_g - \dot{w}_{P,SRC}}{\dot{m}_{SRC}(h_1 - h_4)} \quad (14)$$

where $\dot{w}_{SRC}$ is the net output power of the SRC, $\dot{q}_{SRC}$ is the absorbed heat power of the SRC, and ε_g is the generator efficiency.

The bottoming ORC thermal efficiency is determined by

$$\eta_{ORC} = \frac{\dot{w}_{ORC}}{\dot{q}_{ORC}} = \frac{\dot{w}_{OT}\varepsilon_g - \dot{w}_{P,ORC}}{\dot{m}_{ORC}(h_5 - h_8)} \quad (15)$$

where $\dot{w}_{ORC}$ is the net output power of the ORC, and $\dot{q}_{ORC}$ is the absorbed heat power of the ORC.

The normal SORC thermal efficiency is calculated by

$$\eta_{SORC} = \frac{\dot{w}_{SORC}}{\dot{q}_{SORC}} = \frac{\dot{w}_{SRC} + \dot{w}_{ORC}}{\dot{m}_{SRC}(h_1 - h_4)} \quad (16)$$

where $\dot{w}_{SORC}$ is the net output power of the SORC, and $\dot{q}_{SORC}$ is the absorbed heat power of the SORC, which is equal to $\dot{q}_{SRC}$.

3.6 Operating time of bottoming ORC

For a certain amount of storage water, the operating time of the bottoming ORC in the second-step heat discharge mode is expressed by

$$t_{ORC} = \frac{M_w}{\dot{m}_w} \tag{17}$$

where M_w is the mass of storage water; and $\dot{m}_w$ is derived from Eqs. (10) and (11).

t_{ORC} can represent heat storage capacity as the released heat is used only to drive the bottoming ORC in the second step of the heat discharge process.

3.7 Equivalent heat-to-power efficiency

The equivalent heat-to-power efficiency is defined as

$$\eta_{eq} = \frac{\dot{w}_{total}}{\dot{q}_{total}} = \frac{t_{SORC}\dot{w}_{SORC} + t_{ORC}\dot{w}_{ORC}}{t_{SORC}\dot{q}_{SORC} + t_{ORC}\dot{q}_{ORC}} = \frac{\eta_{SORC} + \tau\gamma\eta_{ORC}}{1+\tau\gamma} \tag{18}$$

$$\gamma = \frac{\dot{q}_{ORC}}{\dot{q}_{SORC}} \tag{19}$$

$$\tau = \frac{t_{ORC}}{t_{SORC}} \tag{20}$$

where t_{SORC} is the operating time of the SORC and is determined according to the duration time of solar radiation; γ is the absorbed heat power ratio between the ORC and the SORC; and τ is the operating time ratio of the ORC and SORC.

η_{eq} comprehensively reflects the performance of the two-stage accumulators-based DSG-SORC system. It is a compromise between η_{SORC} and η_{ORC}. $\tau\gamma$ in weighting factors denotes the heat storage capacity. From the perspective of thermodynamics, η_{eq} indicates how effectively the absorbed solar energy, including that stored in the HTA, is converted into electricity.

4. Results and discussion

In this study, the following assumptions are considered. The main steam and hot water stored in the HTA (T_1) are saturated, and the temperature is supposed to be 250 °C, 260 °C, and 270 °C. The mass of storage water (M_w) is assumed to be 500 ton, 1000 ton, and 1500 ton. Benzene, pentane, and R245fa, which are commonly used in solar ORC power plants [47], are adopted. In addition to the conventional case in which the Baumann factor (*a*) is 1.0, the situations in which *a* equals 0.5 and 1.5 are considered. Other specific parameters and their values are listed in Table 2.

Table 2 Specific parameters for calculation.

Term	**Value**
Rated output power of SORC, $\dot{w}_{SORC}$	10 MW
Reference efficiency of superheated steam turbine, $\varepsilon_{ST,sh}$	85%
ORC dry turbine efficiency, ε_{OT}	85%
Pump efficiency, ε_P	80%
Generator efficiency, ε_g	95%
Operating time of SORC (i.e., duration time of solar radiation), t_{SORC}	8 h
Wind speed, v_w	5 m/s
Ambient temperature, T_a	20 °C
ORC condensation temperature, T_7	30 °C
Minimum temperature difference, ΔT_{min}	10 °C

4.1 Wet steam turbine performance

The exhaust steam wetness (y_2) and wet steam turbine efficiency (ε_{ST}) are determined on the basis of Eqs. (4) to (7). As shown in Figs. 4 and 5, y_2 decreases, whereas ε_{ST} increases with the rise of steam condensation temperature (T_2). This result verifies that the operation environment for the wet steam turbine can be improved by increasing the ORC evaporation temperature. Furthermore, when the main steam temperature (T_1) rises, y_2 increases, whereas ε_{ST} decreases. Given each 10 °C rise in T_1, y_2 increases by approximately 0.67%-1.85%, and ε_{ST} decreases by approximately 0.29%-0.79%. This result is mainly because water is a wet fluid, which means the saturated steam curve in the T-s diagram has a negative slope (Fig. 3). The wet steam turbine is easily subjected to a steam-liquid mixture with the increment of T_1.

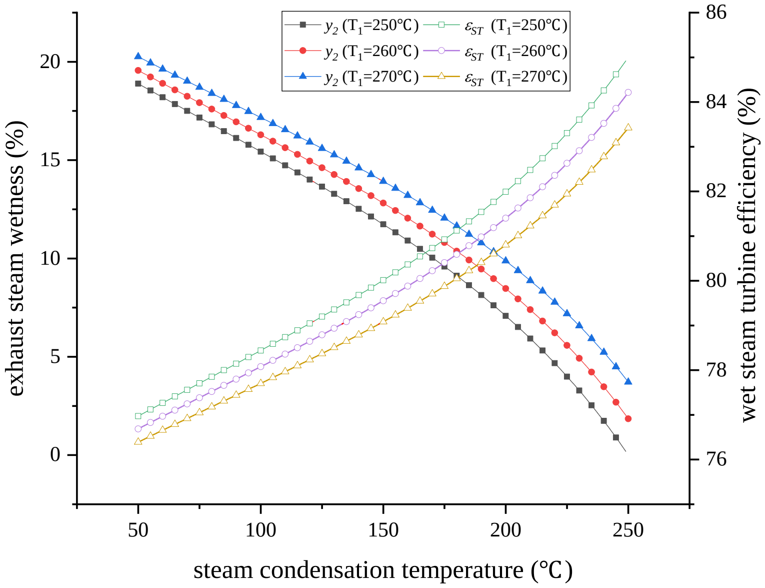

Fig.4 Exhaust steam wetness and wet steam turbine efficiency at a=1.0.

As shown in Fig. 5, y_2 and ε_{ST} increase with the decrement of Baumann factor (a). This finding can be explained as follows: a small a means a weak influence of moisture. Therefore, the wet steam turbine can tolerate a high steam wetness and maintain great efficiency. Moreover, the adverse impacts of a on y_2 and ε_{ST} are reduced at a high T_2, thereby indicating that the technical requirement of moisture separation for the wet steam turbine can be reduced by elevating T_2.

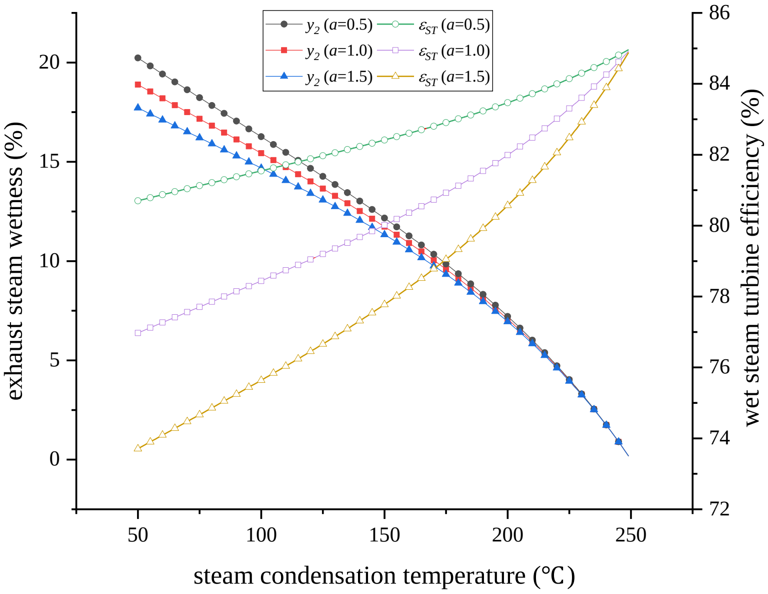

Fig.5 Exhaust steam wetness and wet steam turbine efficiency at T_1=250 °C.

Furthermore, y_2 is generally required to be less than 14% to ensure the reliable and efficient operation of wet steam turbines [11-12]. For different T_1 and a, the values of

T_2 and ε_{ST} at y_2=14% are shown in Table 3. Clearly, the desirable T_2 becomes higher when T_1 increases and *a* decreases. The related ε_{ST} is nearly constant as T_1 rises, but reduces with the elevation of *a*.

Table 3 Values of T_2 and ε_{ST} at y_2=14%.

T_1 (°C)	*a*=0.5		*a*=1.0		*a*=1.5	
	T_2 (°C)	ε_{ST} (%)	T_2 (°C)	ε_{ST} (%)	T_2 (°C)	ε_{ST} (%)
250	128	82.02%	120	79.05%	111	76.08%
260	142	82.03%	134	79.06%	125	76.09%
270	156	82.02%	149	79.05%	140	76.07%

4.2 SRC thermal efficiency

As shown in Fig. 6, the topping SRC thermal efficiency (η_{SRC}) almost linearly decreases with the increment of T_2. Furthermore, when T_1 rises from 250 °C to 270 °C, η_{SRC} elevates by approximately 0.72%-2.82%. As *a* decreases from 1.5 to 0.5, the maximum increment of η_{SRC} is approximately 2.46% at T_2=50 °C. Combined with the results in Part 4.1, the results in the current section show that the SRC does not benefit from the performance improvement of the wet steam turbine at a high T_2. Comparably, the SRC does not suffer from the performance deterioration of the wet steam turbine when T_1 rises. Therefore, compared with *a*, T_1 and T_2 play decisive roles in η_{SRC}.

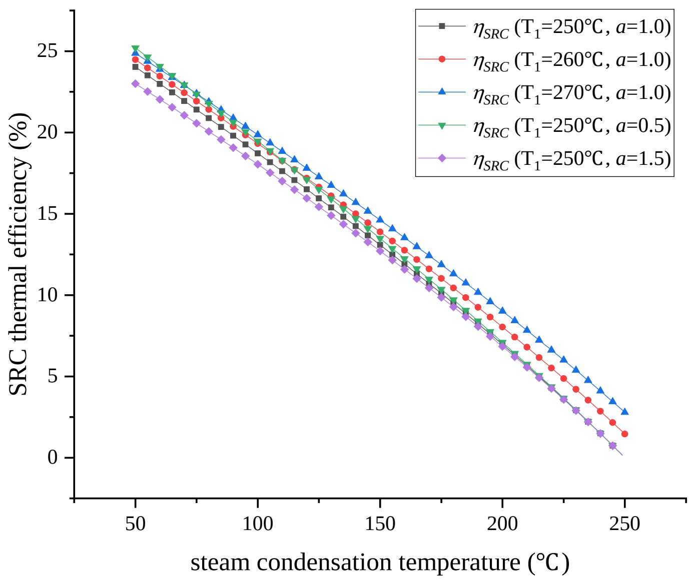

Fig.6 Variations of SRC thermal efficiency.

4.3 ORC performance in heat discharge process

The bottoming ORC thermal efficiency (η_{ORC}) increases when T_2 rises, as shown in Fig. 7. Restricted by critical temperature, the highest T_2 for pentane and R245fa are 206 °C and 164 °C, respectively. Benzene provides the best η_{ORC} owing to the high critical temperature [48-49]. The maximum η_{ORC} of benzene, pentane, and R245fa are 24.33%, 18.14%, and 14.70%, respectively, provided that T_2 in the range of 50-250 °C.

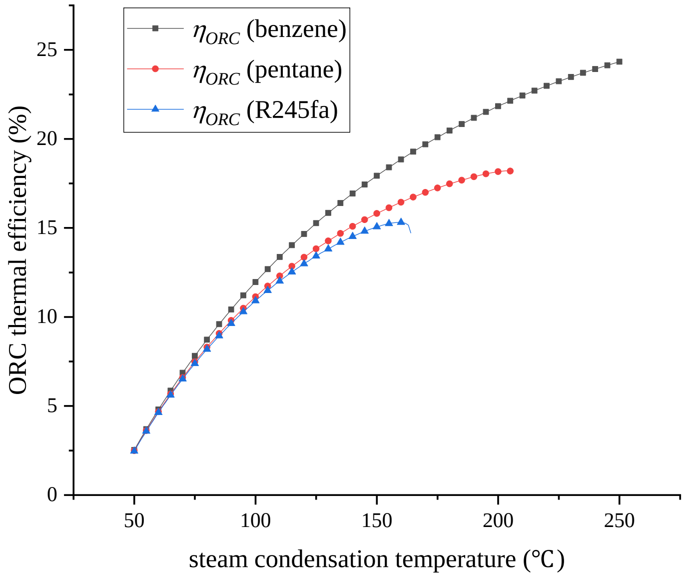

Fig.7 Variations of ORC thermal efficiency.

As shown in Figs. 8 and 9, the operating time of the bottoming ORC (t_{ORC}) increases first and then decreases with the rise of T_2. This result is mainly caused by the opposite variations of the hot water mass flow rate in the heat discharge process ($\dot{m}_w$). By using Eqs. (9) to (11) and (16) to (17), it can be found that

$$t_{ORC} \propto \frac{1}{\dot{m}_w} \propto \frac{1}{\dot{m}_{ORC}} \propto \frac{1}{\dot{m}_{SRC}} \propto \eta_{SORC} \tag{21}$$

Obviously, $\dot{m}_w$ is correlated with the normal SORC thermal efficiency (η_{SORC}), and they have opposite variation. As found in previous studies, η_{SORC} first increases and then decreases with the elevation of ORC evaporation temperature [21-22].

For different ORC fluids, pentane provides a large t_{ORC}, R245fa supplies a moderate t_{ORC}, and benzene delivers a small t_{ORC}, as shown in Fig. 8. This finding is mainly due to the different heat transfer characteristics between organic fluids and water in the intermediate heat exchanger. For pentane and R245fa, the minimum temperature difference occurs in the water outlet. However, it takes place in the pinch point for benzene. The water outlet temperature is higher when benzene is used as ORC working fluid, thereby resulting in a high $\dot{m}_w$. For example, when T_1=250 °C, T_2=150 °C, and a=1.0, $\dot{m}_w$ are approximately 41.50 kg/s for benzene, 30.64 kg/s for pentane, and 31.61 kg/s for R245fa. Moreover, t_{ORC} of benzene decreases significantly if T_2 is close to 250 °C because $\dot{m}_w$ rises up to 130 kg/s or more. For different masses of storage water (M_w), t_{ORC} increases proportionally with the increment of M_w, considering that $\dot{m}_w$ is unvaried. Taking the condition of benzene, T_1=250 °C, T_2=150 °C, and a=1.0 as an example, t_{ORC} is 3.35 h at M_w=500 ton, 6.69 h at M_w=1000 ton, and 10.04 h at M_w=1500 ton.

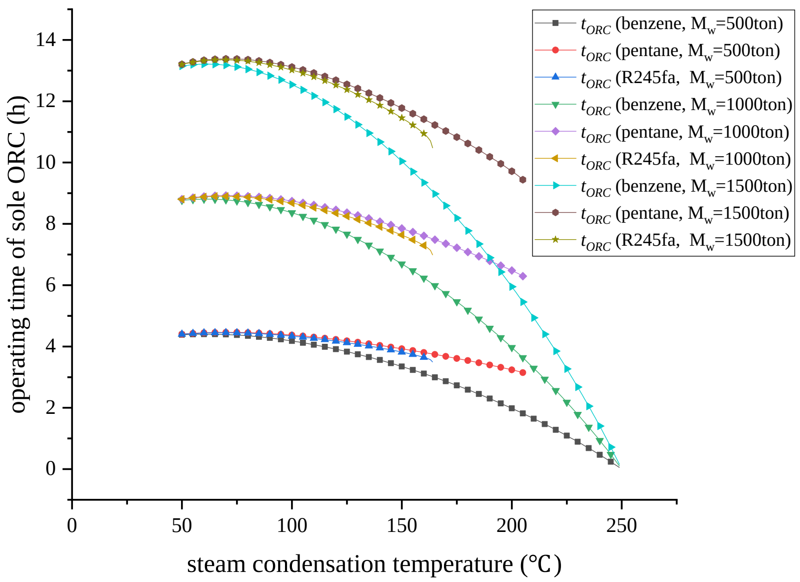

Fig.8 Operating time of bottoming ORC at T_1=250 °C and a=1.0.

As shown in Fig. 9, t_{ORC} almost quantitatively increases with the rise of T_1. Provided that M_w is 500 ton, the increment of t_{ORC} is approximately 0.4-0.6 h for benzene, and 0.4 h for pentane and R245fa when T_1 increases from 250 °C to 260 °C or rises from 260 °C to 270 °C. t_{ORC} increases as a decreases. Furthermore, the effect of a on t_{ORC} is becoming significant when T_2 is close to 50 °C, but becomes negligible as T_2 approaches a high value, such as 175 °C for benzene. The main reason is that the beneficial effect of a small a on η_{SRC} is reduced with the increment of T_2 (Fig. 6), thereby resulting in a hot water mass flow rate which is similar to that under a high a. For example, when T_1=250 °C and T_2=175 °C, $\dot{m}_w$ of benzene are 50.35, 50.86 and 51.35 kg/s, respectively, as a is equal to 0.5, 1.0, and 1.5.

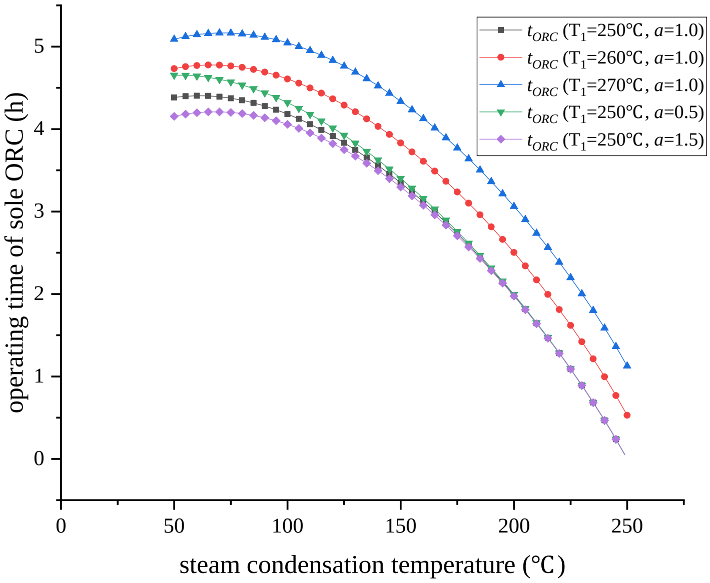

Fig.9 Operating time of bottoming ORC for benzene at M_w=500 ton.

4.4 Solar collector efficiency

In this study, the solar collector efficiency (η_{col}) decreases slightly with the increments of T_1 and T_2. For a given direct normal solar irradiance (I_{DN}) of 800 W/m^2, η_{col} is approximately 76.1% when T_1=250 °C and T_2=50 °C, and drops to 75.1% at T_1=270 °C and T_2=250 °C, as shown in Fig. 10. The main reason for this finding is because the average heat loss from the evacuated tube receivers ($q_{loss,av}$) is low at a low-medium collection temperature. Specifically, $q_{loss,av}$ is only approximately 30-74 W/m^2 in the proposed system, which is 1/5-1/2 of that in oil or molten salt-based solar thermal power plants [45, 50]. Moreover, solar irradiation also has a negligible effect on η_{col} in the proposed system. The maximum decrement of η_{col} is just approximately 1.5% when I_{DN} declines from 800 W/m^2 to 400 W/m^2. The minor variations in solar collector efficiency in the low-medium temperature range are consistent with those in previous studies. [43, 51-52]. Therefore, it is reasonable to ignore the influence of η_{col} on system performance in the next evaluation of equivalent heat-to-power efficiency.

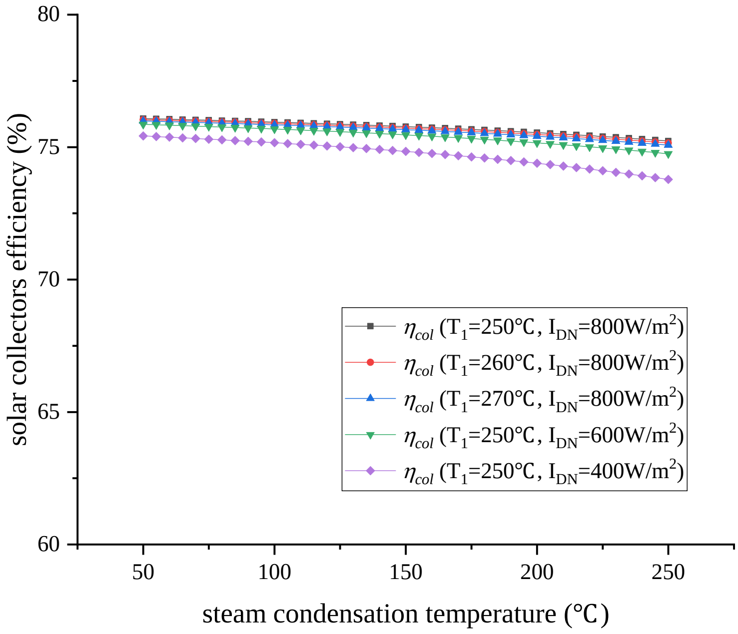

Fig.10 Variations of solar collector efficiency.

4.5 Equivalent heat-to-power efficiency

Similar to η_{SORC}, the equivalent heat-to-power efficiency (η_{eq}) increases first and then decreases with the rise of T_2, as shown in Figs. 12 and 13. However, the optimum steam condensation temperature ($T_{2,opt}$) that corresponds to the maximum η_{eq} ($\eta_{eq,max}$) is higher than that ($T'_{2,opt}$) based on the maximum η_{SORC} ($\eta_{SORC,max}$). Take the case of benzene, T_1=250 °C, a=1.0, and M_w=500 ton as an example, $T_{2,opt}$ and $T'_{2,opt}$ are 187 °C and 132 °C, respectively. Given that η_{eq} comprehensively considers the efficiencies of the cascade SORC and the sole ORC operating in the heat discharge process, the impact of η_{ORC} on η_{eq} is more significant than that on η_{SORC}. This finding can be derived in theory as follows.

η_{SORC} can be presented as

$$\eta_{SORC} = \frac{\dot{w}_{SORC}}{\dot{q}_{SORC}} = \frac{\dot{w}_{SRC}+\dot{w}_{ORC}}{\dot{q}_{SORC}} = \frac{\dot{q}_{SORC}\eta_{SRC}+\gamma\dot{q}_{SORC}\eta_{ORC}}{\dot{q}_{SORC}} = \eta_{SRC} + \gamma\eta_{ORC} \tag{22}$$

where the coefficient ratio between η_{ORC} and η_{SRC} is

$$\frac{\mathrm{C}(\eta_{ORC})}{\mathrm{C}(\eta_{SRC})} = \gamma \tag{23}$$

η_{eq} can be presented as

$$\eta_{eq} = \frac{\eta_{SORC}+\tau\gamma\eta_{ORC}}{1+\tau\gamma} = \frac{\eta_{SRC}+\gamma\eta_{ORC}+\tau\gamma\eta_{ORC}}{1+\tau\gamma} = \frac{1}{1+\tau\gamma}\eta_{SRC} + \frac{\gamma+\tau\gamma}{1+\tau\gamma}\eta_{ORC} \tag{24}$$

where the coefficient ratio between η_{ORC} and η_{SRC} is

$$\frac{\mathrm{C}(\eta_{ORC})}{\mathrm{C}(\eta_{SRC})} = \gamma(1+\tau) \tag{25}$$

because

$$\gamma > 0 \tag{26}$$

$$\tau > 0 \tag{27}$$

therefore

$$\gamma(1+\tau) > \gamma \tag{28}$$

A high T_2 delivers an improved η_{ORC} ; thus, $T_{2,opt}$ is larger than $T'_{2,opt}$.

The effects of T_2 on the absorbed heat power ratio (γ) and the operating time ratio (τ) are presented in Fig.11. γ increases when T_2 rises, primarily because the absorbed heat power of the ORC ($\dot{q}_{ORC}$) increases. Take for example, benzene, T_1=250 °C, and a=1.0. $\dot{q}_{ORC}$ is 28.82 MW at T_2=50 °C, and 30.21 MW at T_2=150 °C. The variations of τ with T_2 are similar to those of t_{ORC} considering that t_{SORC} is set as a constant.

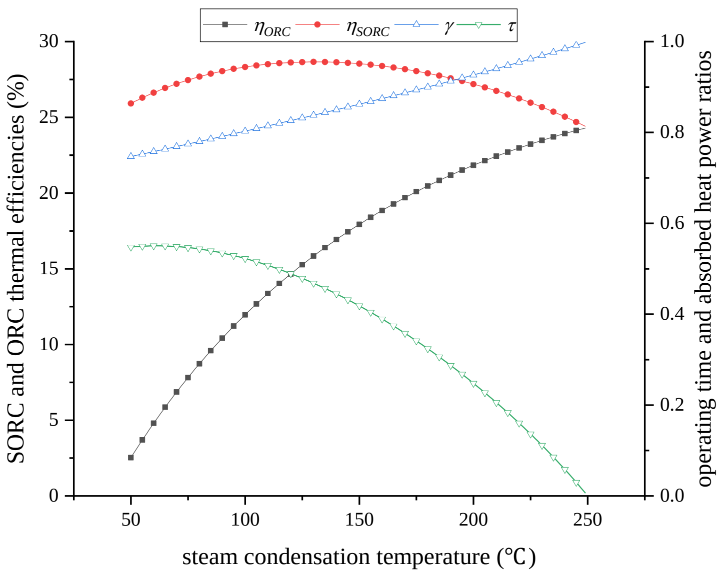

(a)

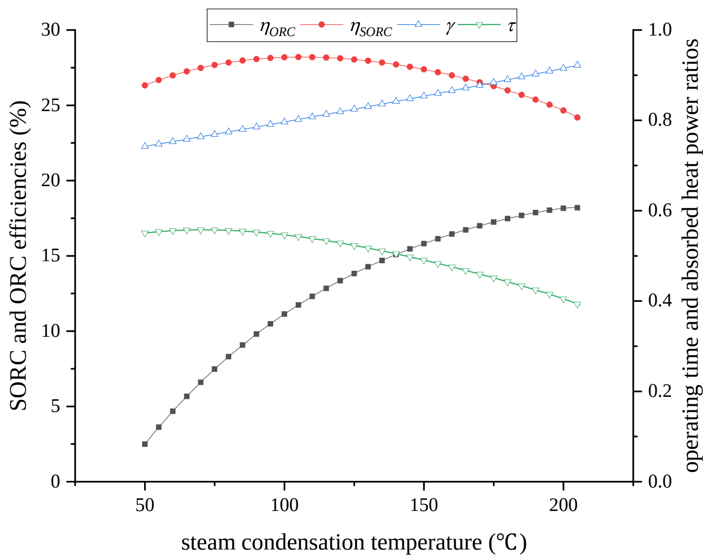

(b)

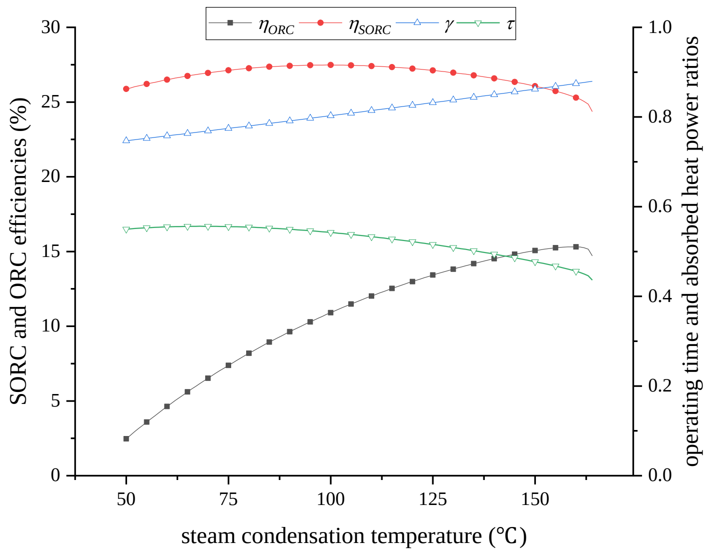

(c)

Fig.11 Parameters related with η_{eq} at M_w=500 ton, T_1=250 °C and a=1.0: (a) benzene; (b) pentane; (c) R245fa.

Compared with pentane and R245fa, benzene provides the best η_{eq} and the highest $T_{2,opt}$, as shown in Fig.12. Because η_{ORC} is high when using benzene as ORC fluid (Part 4.3). Specifically, $\eta_{eq,max}$ and $T_{2,opt}$ are 25.19%-27.11% and 185-239 °C for benzene, 20.93%-24.24% and 139-190 °C for pentane, and 19.89%-23.75% and 131-154 °C for R245fa. Furthermore, when M_w increases from 500 ton to 1500 ton, the impact of η_{ORC} on η_{eq} is enhanced due to the increment of t_{ORC}, thereby resulting in a decrease of η_{eq} and increase in $T_{2,opt}$. For example, in the case of benzene,

T_1=250 °C and a=1.0, $\eta_{eq,max}$ and $T_{2,opt}$ are, respectively, 26.25% and 187 °C at M_w=500 ton and vary to 25.22% and 220 °C at M_w=1500 ton.

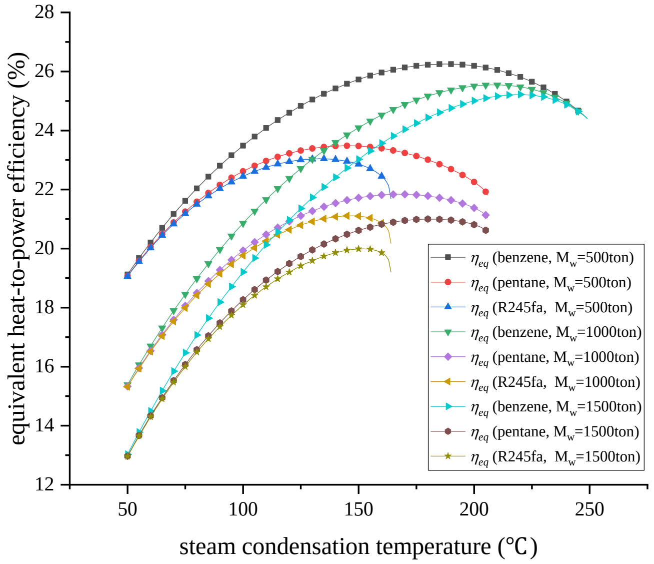

Fig.12 Equivalent heat-to-power efficiency at T_1=250 °C and a=1.0.

As shown in Fig. 13, η_{eq} rises with the increment of T_1 considering that η_{SRC} is improved. $T_{2,opt}$ also elevates when T_1 increases. However, the main reason is that the impact of η_{ORC} on η_{eq} is strengthened because of the increase of t_{ORC} (Fig. 9). Differently, as a becomes small, η_{eq} increases, whereas $T_{2,opt}$ slightly decreases because the values of t_{ORC} nearby $T_{2,opt}$ are almost unvaried, whereas η_{SRC} is increased when a decreases, thereby resulting in the weak impact of η_{ORC} on η_{eq} (Figs. 6 and 9).

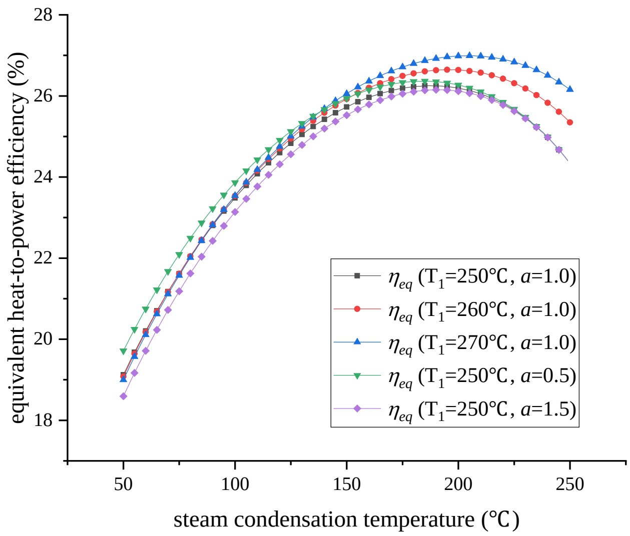

Fig.13 Equivalent heat-to-power efficiency for benzene at M_w=500 ton.

The parameter values corresponding to $\eta_{eq,max}$ at different conditions are shown in Tables 4 to 6. Generally, these parameters are reasonable. Notably, y_2 sometimes exceeds 14% for pentane and R245fa, especially when M_w=500 ton, T_1=260-270 °C and a =0.5-1.0. From this perspective, benzene is compliant, whereas pentane and R245fa are suitable for the system with high M_w and superior moisture separation technology. Furthermore, the water temperature in the LTA (T_{LTA}) is close to the theoretical minimum (i.e., 40 °C) for pentane and R245fa at $\eta_{eq,max}$. Thus, the stored hot water is fully used. Although the T_{LTA} of benzene is higher than 115 °C at $\eta_{eq,max}$, it is beneficial to avoid highly inefficient utilization of the stored water. Otherwise, a poor ORC efficiency of less than 5% is inevitable if the T_{LTA} of benzene approaches 40 °C. Considering t_{ORC} and η_{eq}, pentane is a preferable ORC fluid by comparison with benzene and R245fa.

Table 4 Parameters that corresponds to $\eta_{eq,max}$ at a=0.5.

ORC fluid	T_1 **(°C)**	M_w **(ton)**	$\eta_{eq,max}$ **(%)**	η_{SORC} **(%)**	η_{ORC} **(%)**	$T_{2,opt}$ **(°C)**	y_2 **(%)**	T_{LTA} **(°C)**	t_{ORC} **(h)**
Benzene	**250**	**500**	26.37	27.91	20.83	185	8.85	120.8	2.47
		1000	25.60	26.97	22.26	207	6.39	153.0	3.51
		1500	25.24	26.29	22.98	220	4.73	176.7	3.86
	260	**500**	26.76	28.47	21.32	192	9.49	118.6	2.78
		1000	25.96	27.38	22.82	217	6.69	155.9	3.86
		1500	25.60	26.74	23.43	229	5.12	178.7	4.39
	270	**500**	27.11	28.95	21.83	200	10.12	116.3	3.09
		1000	26.28	27.80	23.28	226	7.19	155.6	4.34
		1500	25.91	27.21	23.80	237	5.71	177.0	5.16
Pentane	**250**	**500**	23.71	27.50	15.02	139	13.11	40.5	4.13
		1000	21.95	26.24	16.79	166	10.72	40.9	7.56
		1500	21.07	25.40	17.48	180	9.36	41.1	10.73
	260	**500**	23.99	27.89	15.61	147	13.56	40.6	4.41
		1000	22.18	26.86	16.95	169	11.69	40.9	8.20

		1500	21.27	25.97	17.64	184	10.29	41.2	11.62
	270	**500**	24.24	28.44	15.81	150	14.49	40.6	4.75
		1000	22.37	27.32	17.20	174	12.54	41.0	8.80
		1500	21.44	26.49	17.80	188	11.29	41.3	12.54
R245fa	**250**	**500**	23.31	27.38	13.90	131	13.78	40.9	4.16
		1000	21.27	26.71	14.82	145	12.60	41.2	7.93
		1500	20.10	26.27	15.15	152	11.99	41.4	11.56
	260	**500**	23.55	27.98	14.05	133	14.68	40.9	4.50
		1000	21.41	27.32	14.92	147	13.56	41.3	8.60
		1500	20.20	27.01	15.15	152	13.15	41.4	12.66
	270	**500**	23.75	28.44	14.33	137	15.48	41.0	4.83
		1000	21.52	27.81	15.06	150	14.49	41.3	9.26
		1500	20.26	27.55	15.22	154	14.18	41.4	13.68

Table 5 Parameters that corresponds to $\eta_{eq,max}$ at a=1.0.

ORC fluid	T_1 **(°C)**	M_w **(ton)**	$\eta_{eq,max}$ **(%)**	η_{SORC} **(%)**	η_{ORC} **(%)**	$T_{2,opt}$ **(°C)**	y_2 **(%)**	T_{LTA} **(°C)**	t_{ORC} **(h)**
Benzene	**250**	**500**	26.25	27.69	20.98	187	8.44	123.4	2.39
		1000	25.55	26.89	22.26	207	6.29	153.0	3.50
		1500	25.22	26.25	22.98	220	4.67	176.7	3.85
	260	**500**	26.65	28.17	21.58	196	8.87	123.8	2.63
		1000	25.91	27.21	22.93	219	6.34	159.4	3.69
		1500	25.57	26.70	23.43	229	5.06	178.7	4.38
	270	**500**	26.99	28.63	22.08	204	9.49	121.5	2.94
		1000	26.23	27.57	23.43	229	6.70	161.1	4.09
		1500	25.88	27.05	23.88	239	5.37	181.3	4.89
Pentane	**250**	**500**	23.48	26.90	15.46	145	12.13	40.6	3.98
		1000	21.84	25.94	16.84	167	10.31	40.9	7.43
		1500	21.00	25.21	17.48	180	9.12	41.1	10.62
	260	**500**	23.76	27.38	15.81	150	12.81	40.6	4.28

		1000	22.06	26.32	17.20	174	10.90	41.0	7.95
		1500	21.19	25.64	17.23	186	9.83	41.2	11.41
	270	**500**	23.99	27.85	16.08	154	13.64	40.7	4.59
		1000	22.24	26.86	17.34	177	11.89	41.0	8.58
		1500	21.35	26.19	17.84	189	10.88	41.3	12.33
R245fa	**250**	**500**	23.04	26.87	14.05	133	13.06	40.9	4.04
		1000	21.11	26.24	14.92	147	11.97	41.3	7.72
		1500	19.99	25.94	15.15	152	11.57	41.4	11.36
	260	**500**	23.27	27.34	14.33	137	13.77	41.0	4.34
		1000	21.25	26.80	15.02	149	12.89	41.3	8.36
		1500	20.08	26.50	15.22	154	12.51	41.4	12.31
	270	**500**	23.46	27.81	14.52	140	14.61	41.1	4.67
		1000	21.34	27.36	15.06	150	13.92	41.3	9.05
		1500	20.13	27.12	15.22	154	13.64	41.4	13.38

Table 6 Parameters that corresponds to $\eta_{eq,max}$ at a=1.5.

ORC fluid	T_1 (°C)	M_w (ton)	$\eta_{eq,max}$ (%)	η_{SORC} (%)	η_{ORC} (%)	$T_{2,opt}$ (°C)	y_2 (%)	T_{LTA} (°C)	t_{ORC} (h)
Benzene	**250**	**500**	26.15	27.42	21.25	191	7.86	128.8	2.25
		1000	25.50	26.59	22.55	212	5.60	161.6	3.14
		1500	25.19	26.21	22.98	220	4.62	176.7	3.84
	260	**500**	26.54	27.95	21.71	198	8.48	126.5	2.55
		1000	25.87	27.09	22.98	220	6.12	161.2	3.61
		1500	25.55	26.60	23.48	230	4.87	180.7	4.25
	270	**500**	26.89	28.38	22.26	207	8.99	125.5	2.82
		1000	26.18	27.50	23.43	229	6.60	161.1	4.07
		1500	25.86	27.01	23.88	239	5.31	181.3	4.88
Pentane	**250**	**500**	23.28	26.47	15.67	148	11.48	40.6	3.88
		1000	21.74	25.62	16.95	169	9.84	40.9	7.29
		1500	20.93	24.80	17.64	184	8.53	41.2	10.36

	260	**500**	23.55	26.90	16.08	154	12.07	40.7	4.16
		1000	21.95	26.03	17.25	175	10.50	41.0	7.82
		1500	21.12	25.44	17.72	186	9.58	41.2	11.29
	270	**500**	23.77	27.37	16.26	157	12.94	40.7	4.47
		1000	22.13	26.43	17.48	180	11.30	41.1	8.37
		1500	21.28	25.90	17.87	190	10.51	41.3	12.14
R245fa	**250**	**500**	22.80	26.40	14.19	135	12.41	41.0	3.93
		1000	20.96	25.91	14.92	147	11.55	41.3	7.59
		1500	19.89	25.64	15.15	152	11.18	41.4	11.18
	260	**500**	23.02	26.81	14.52	140	13.02	41.1	4.21
		1000	21.09	26.38	15.06	150	12.35	41.3	8.18
		1500	19.97	26.16	15.22	154	12.07	41.4	12.09
	270	**500**	23.19	27.34	14.52	140	14.01	41.1	4.56
		1000	21.18	26.84	15.15	152	13.26	41.4	8.80
		1500	20.01	26.73	15.22	154	13.14	41.4	13.11

4.6 Comparison with the design based on the SORC efficiency

Notably, the design T_2 based on η_{eq} results in a more cost-effective solar thermal power system than that based on the efficiency of the sole power conversion mode i.e., η_{SORC}. Given the size of the accumulators and power block capacity (i.e., M_w and $\dot{w}_{SORC}$), the solar collector area designed for the charge process is approximately constant because of the similar heat releases in the discharge process. The collector area designed for normal operating conditions varies with η_{SORC}. As shown in Table 7, in the case of T_2=$T_{2,opt}$, η_{SORC} is low and the collector area designed for the normal operating conditions needs to be large. Therefore, the total collector areas of the proposed system with a design T_2=$T_{2,opt}$ are larger than that with T_2=$T'_{2,opt}$. For the former, additional solar collectors are used, but the overall solar thermal electricity efficiency is high. Thus, additional annual power yield can be achieved, whereas the additional investment is only made in solar collectors. The payback time of the system is consequently short.

Table 7 η_{eq}, η_{SORC}, and T_2 that corresponds to $\eta_{eq,max}$ and $\eta_{SORC,max}$ of pentane at M_w=1500 ton.

		η_{eq}=$\eta_{eq,max}$			η_{SORC}=$\eta_{SORC,max}$		
a	**T_1 (°C)**	**$\eta_{eq,max}$ (%)**	**η_{SORC} (%)**	**$T_{2,opt}$ (°C)**	**η_{eq} (%)**	**$\eta_{SORC,max}$ (%)**	**$T'_{2,opt}$ (°C)**
0.5	**250**	21.07	25.40	180	18.23	28.32	97
	260	21.27	25.97	184	18.17	28.91	97
	270	21.44	26.49	188	18.31	29.45	100
1.0	**250**	21.00	25.21	180	18.48	27.66	103
	260	21.19	25.64	186	18.70	28.21	107
	270	21.35	26.19	189	18.77	28.70	109
1.5	**250**	20.93	24.80	184	18.84	27.11	111
	260	21.12	25.44	186	18.92	27.62	113
	270	21.28	25.90	190	19.05	28.07	116

4.7 Sensitivity analysis

In the above analysis, emphasis is placed on the impacts of the main steam temperature (T_1), Baumann factor (a), mass of storage water (M_w), and ORC working fluid on the equivalent heat-to-power efficiency (η_{eq}). The results indicate that η_{eq} is sensitive to these four parameters. Other parameters include the system power capacity, device efficiencies, SORC operation time (t_{SORC}), ambient temperature (T_a), and minimum temperature difference (ΔT_{min}) are assumed to be constant, as listed in Table 2.

The rated output power of 10 MW is appropriate, considering that the commercial solar thermal power plants usually have the same power capacity, such as the Planta Solar 10 [5], Shouhang Dunhuang 10 MW Phase I [53], and Supcon Delingha 10 MW Phase I [54]. The rated output power should not have an effect on the design of the steam condensation temperature because the working fluid mass flow rate and tank volume can vary proportionally with the output power. More important, the design methodology remains applicable. Furthermore, 85% design efficiency of the reference superheated steam turbine and ORC dry turbine has been reported [3, 55-56]. In conventional fossil fuel power plants, the reheat turbine of superheated steam generally has an efficiency of approximately 85%-94% [20]. The multistage turbines in the ORC field commonly have an isentropic efficiency of 80%-90% [19, 47]. Therefore, the possibility of a significant deviation in device efficiencies in a practical solar thermal power plant from the assumed values is low.

Unlike the device efficiencies, t_{SORC}, T_a, and ΔT_{min} may change with the local meteorological conditions. The sensitivity analysis of these three factors on η_{eq} is necessary. The influence of t_{SORC} on η_{eq} is shown in Fig.14 (a). Pentane is used as the ORC fluid. T_1=250 °C, a=1.0, and M_w=1500 ton. The other parameters are the same as those listed in Table 2. η_{eq} declines, whereas $T_{2,opt}$ increases with the decrement of t_{SORC}. For example, $\eta_{eq,max}$ drops from 21.45% to 20.49% when t_{SORC} decreases from 10 h to 6 h, with a corresponding $T_{2,opt}$ from 174 °C to 189 °C. T_a has appreciable influence on η_{eq}, as shown in Fig.14 (b). T_a is related to the ORC condensation temperature, thereby influencing the ORC and SORC efficiencies. $\eta_{eq,max}$ increases from 19.98% to 22.06% when T_a decreases from 30 °C to 10 °C. However, $T_{2,opt}$ only has a variation of 2 °C. ΔT_{min} also affect η_{eq}. A larger ΔT_{min} leads to greater irreversibility in the heat exchangers and lower power efficiency. As shown in Fig.2 (c), $\eta_{eq,max}$ declines from 21.14% to 20.85% and $T_{2,opt}$ increases from 178 °C to 184 °C as ΔT_{min} rises from 5 °C to 15 °C.

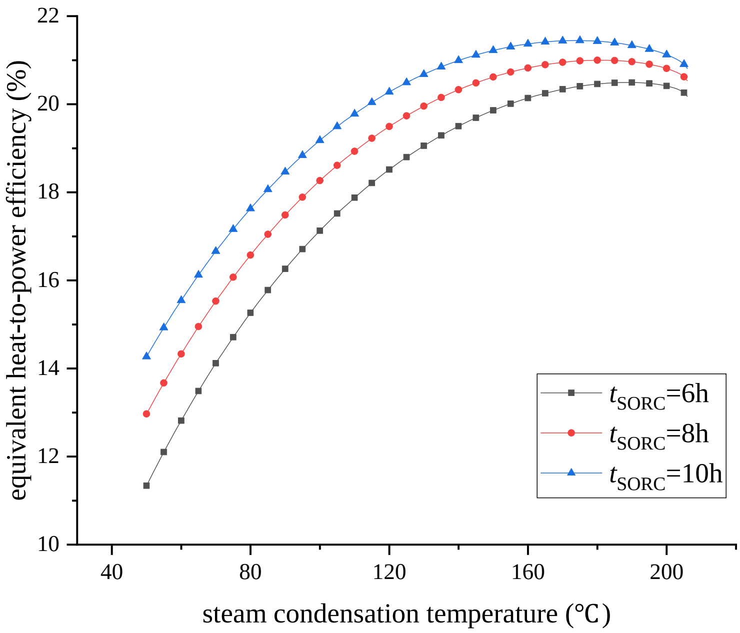

(a)

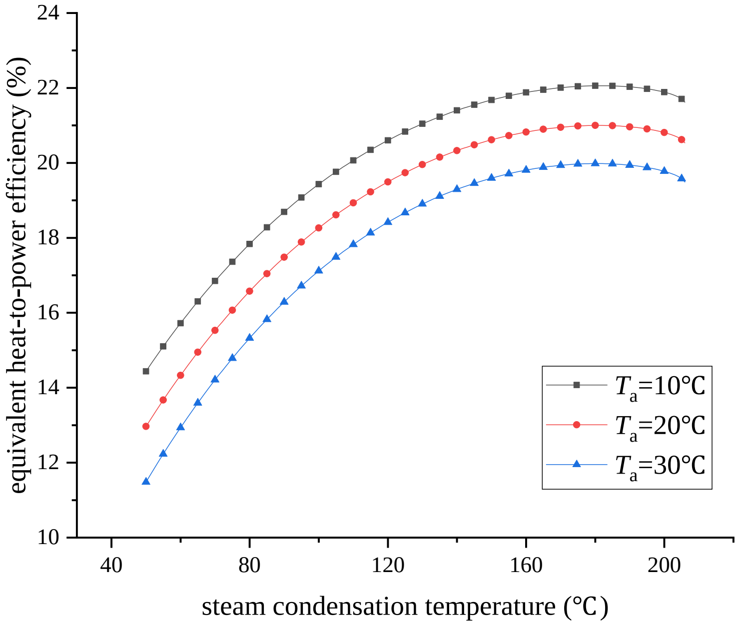

(b)

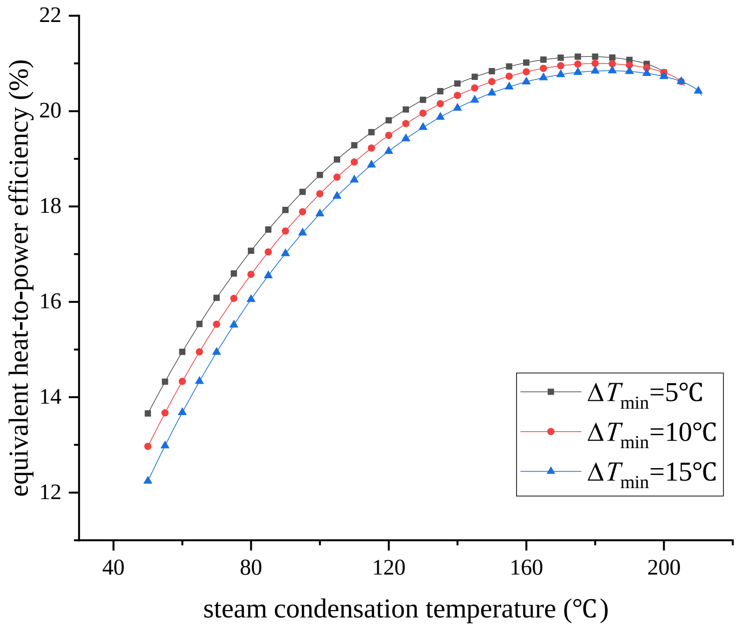

(c)

Fig.14 Variations of equivalent heat-to-power efficiency in the case of pentane, T_1=250 °C, a=1.0, and M_w=1500 ton (a) t_{SORC}; (b) T_a; (c) ΔT_{min}.

Notably, solar energy resource is important in the design of the steam condensation temperature, although it does not exert a direct influence on η_{eq}. The reason is that t_{SORC} is closely related to the local solar energy resource. Figure 14 (a) indicates that $\eta_{eq,max}$ increases and $T_{2,opt}$ decreases with the increment of t_{SORC}. In regions with abundant solar energy, t_{SORC} is expected to be high. A possible relationship between solar radiation and t_{SORC} is shown in Fig.15. The solar radiation variations in a typical day for two regions are shown. $I_{DN,critical}$ represents the solar irradiation at which the heat collected from the solar field is equal to that consumed by the SORC. Power is generated by the SORC during the period from t to $t + t_{SORC}$, but by ORC for the rest of the day (24-t_{SORC}). The area in red represents the total heat consumption by the SORC when multiplied by the collector efficiency and surface area, and that in blue represents the total heat stored and used for the ORC. Assuming the solar collectors can provide sufficient heat for the 24 h power generation, t_{SORC} should fulfil Eq.(29). Obviously, t_{SORC} is associated with the local solar radiation.

$$\frac{\dot{q}_{SORC}\times t_{SORC}}{\dot{q}_{ORC}\times(24-t_{SORC})} = \frac{A_{red}}{A_{blue}} \tag{29}$$

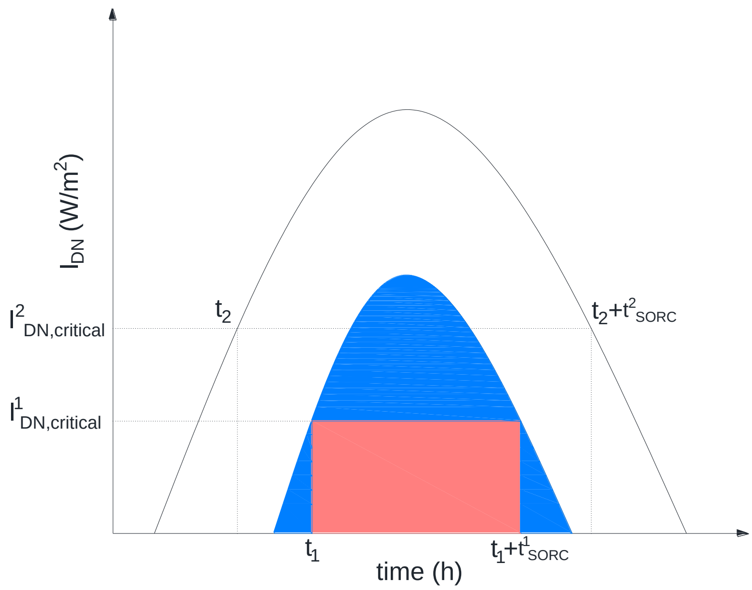

Fig.15 Variations of t_{SORC} with solar irradiation.

5. Conclusions

An innovative solar thermal power generation system using cascade SORC and two-stage accumulators has recently been proposed. The system offers a significantly higher heat storage capacity than conventional direct steam generation (DSG) solar power plants. The steam condensation temperature (T_2) in the proposed system is a crucial parameter because it affects the SORC efficiency (η_{SORC}) in normal operations and the power conversion of the bottoming ORC in the unique heat discharge process. This article develops a methodology for the design of T_2 with respect to a new indicator, namely, the equivalent heat-to-power efficiency (η_{eq}). η_{eq} is a compromise between the efficiencies in different operation modes. The effects of main steam temperature (T_1), Baumann factor (a), mass of storage water (M_w), and ORC working fluid on T_2 are investigated. The results show the following:

(1) The wet steam turbine efficiency (ε_{ST}) rises with the increase in T_2 and decrease in a. However, ε_{ST} reduces as T_1 increases. To guarantee the reliable operation of the wet steam turbine, T_2 needs to be higher than 111-156 °C, provided that T_1 ranges between 250 °C and 270 °C, and a varies from 0.5 to 1.5.

(2) The SRC thermal efficiency (η_{SRC}) increases when T_1 rises and T_2 and a reduce. Compared with a, T_1 and T_2 play decisive roles in η_{SRC}.

(3) The ORC thermal efficiency (η_{ORC}) rises when T_2 increases. The operating time of the bottoming ORC in the heat discharge process (t_{ORC}) first increases and then decreases as T_2 rises. To obtain a higher t_{ORC}, a large T_1 and M_w as well as a small a are preferable. For different ORC fluids, benzene delivers the best η_{ORC}, whereas pentane provides the highest t_{ORC}.

(4) η_{eq} is a better indicator than η_{SORC}. The optimum steam condensation temperature ($T_{2,opt}$) that corresponds to the maximum η_{eq} ($\eta_{eq,max}$) is generally higher than that based on the maximum η_{SORC}. $T_{2,opt}$ reduces as T_1, and a and M_w decrease. $\eta_{eq,max}$ rises with the increment of T_1 and the decrement of a and M_w. Benzene is compliant, whereas pentane and R245fa are suitable for the system with high M_w and superior moisture separation technology. Considering t_{ORC} and η_{eq}, pentane is a preferable ORC fluid, and the corresponding $T_{2,opt}$ and $\eta_{eq,max}$ are respectively 139-190 °C and 20.93%-24.24%, provided that T_1 ranges between 250 °C and 270 °C, a varies from 0.5 to 1.5, and M_w changes from 500 ton to 1500 ton.

Acknowledgments

The study was sponsored by the EU Marie Curie International Incoming Fellowships Program (703746), National Science Foundation of China (NSFC 51476159, 51761145109, 51776193), and International Technology Cooperation Program of the Anhui Province of China (BJ2090130038).

References

[1] Giglio A, Lanzini A, Leone P, García MMR, Moya EZ. Direct steam generation in parabolic-trough collectors: A review about the technology and a thermo-economic analysis of a hybrid system. Renew Sust Energ Rev 2017;74:453-73. doi: 10.1016/j.rser.2017.01.176.

[2] Eck M, Zarza E, Eickhoff M, Rheinländer J, Valenzuela L. Applied research concerning the direct steam generation in parabolic troughs. Sol Energy 2003;74:341-51. doi: 10.1016/S0038-092X(03)00111-7.

[3] Elsafi AM. Exergy and exergoeconomic analysis of sustainable direct steam generation solar power plants. Energy Conv Manag 2015;103:338-47. doi: 10.1016/j.enconman.2015.06.066.

[4] NREL. Concentrating Solar Power Projects by Technology, http://www.nrel.gov/csp/solarpaces/by_technology.cfm; [accessed 25 May 2018].

[5] Osuna R, Olavarría R, Morillo R, Sánchez M, Cantero F, Fernández-Queroa V, Robles P, López del Cerro T, Esteban A, Cerón F, Talegón J, Romero M, Téllez F, Marcos M, Martínez D, Valverde A, Monterreal R, Pitz-Paal R, Brakmann G, Ruiz V, Silva M, Menna P. Ps10, Construction of a 11MW Solar Thermal Tower Plant in Seville, Spain. SolarPaces 2006.

[6] Puerto Errado 2, http://www.puertoerrado2.com/projekt/kraftwerk/; 2013 [accessed 25 May 2018].

[7] Siemens. Steam turbines for CSP plants, http://m.energy.siemens.com/hq/pool/hq/power-generation/steam-turbines/downloads/steam-turbine-for-csp-plants-siemens.pdf; 2011 [accessed 25 May 2018].

[8] González-Roubaud E, Pérez-Osorio D, Prieto C. Review of commercial thermal energy storage in concentrated solar power plants: Steam vs. molten salts. Renew Sust Energ Rev 2017;80:133–48. doi:10.1016/j.rser.2017.05.084.
[9] Baumann K. Some recent developments in large steam turbine practice. Engineer 1921;111:435-58.
[10] Vatanmakan M, Lakzian E, Mahpeykar MR. Investigating the entropy generation in condensing steam flow in turbine blades with volumetric heating. Energy 2018;147:701-14. doi: 10.1016/j.energy.2018.01.097.
[11] Hirsch T, Khenissi A. A systematic comparison on power block efficiencies for CSP plants with direct steam generation. Energy Procedia 2014;49:1165-76. doi:10.1016/j.egypro.2014.03.126.
[12] Xu L, Yuan JQ. Online application oriented calculation of the exhaust steam wetness fraction of the low pressure turbine in thermal power plant. Appl Therm Eng 2015;76:357-66. doi: 10.1016/j.applthermaleng.2014.11.020.
[13] Steinmann WD, Eck M. Buffer storage for direct steam generation. Sol Energy 2006;80:1277–82. doi:10.1016/j.solener.2005.05.013.
[14] Casati E, Galli A, Colonna P. Thermal energy storage for solar-powered organic Rankine cycle engines. Sol Energy 2013;96:205-19. doi:10.1016/j.solener.2013.07.013.
[15] Beckmann G, Gilli PV. Thermal Energy Storage. Verlag Wien: Springer; 1984.
[16] Prieto C, Rodríguez A, Patiño D, Cabeza LF. Thermal energy storage evaluation in direct steam generation solar plants. Sol Energy 2018;159:501-9. doi:10.1016/j.solener.2017.11.006.
[17] Li J, Gao GT, Pei G, Li PC, Su YH, Ji J, Riffat S. A novel concentrated solar power system using cascade steam organic Rankine cycle and two-stage accumulators. Energy Procedia 2017;142:386-94. doi: 10.1016/j.egypro.2017.12.061.
[18] Dincer I, Demir ME. Steam and Organic Rankine Cycles. Comprehensive Energy Systems 2018;4:264-311. doi:10.1016/B978-0-12-809597-3.00410-7.
[19] Turboden. Turboden ORC Technology, http://www.turboden.com/turboden-orc-technology/1065/innovation; [accessed 25 May 2018].
[20] Leyzerovich A. Wet-Steam Turbines for Nuclear Power Plants. American ed.

PennWell Corp; 2015.

[21] Li J, Li PC, Pei G, Alvi JZ, Ji J. Analysis of a novel solar electricity generation system using cascade Rankine cycle and steam screw expander. Appl Energy 2016;165:627-38. doi:10.1016/j.apenergy.2015.12.087.

[22] Li PC, Li J, Gao GT, Pei G, Su YH, Ji J, Ye B. Modeling and optimization of solar-powered cascade Rankine cycle system with respect to the characteristics of steam screw expander. Renew Energy 2017;112:398-412. doi:10.1016/j.renene.2017.05.054.

[23] Liu B, Riviere P, Coquelet C, Gicquel R, David F. Investigation of a two stage Rankine cycle for electric power plants. Appl Energy 2012;100:285-94. doi:10.1016/j.apenergy.2012.05.044.

[24] Ziółkowski P, Kowalczyk T, Kornet S, Badura J. On low-grade waste heat utilization from a supercritical steam power plant using an ORC-bottoming cycle coupled with two sources of heat. Energy Conv Manag 2017;146:158-73. doi: 10.1016/j.enconman.2017.05.028.

[25] Choi BC, Kim YM. Thermodynamic analysis of a dual loop heat recovery system with trilateral cycle applied to exhaust gases of internal combustion engine for propulsion of the 6800 TEU container ship. Energy 2013;58:404-16. doi: 10.1016/j.energy.2013.05.017.

[26] Nazari N, Heidarnejad P, Porkhial S. Multi-objective optimization of a combined steam-organic Rankine cycle based on exergy and exergo-economic analysis for waste heat recovery application. Energy Conv Manag 2016;127:366-79. doi:10.1016/j.enconman.2016.09.022.

[27] Shu GQ, Liu LN, Tian H, Wei HQ, Liang YC. Analysis of regenerative dual-loop organic Rankine cycles (DORCs) used in engine waste heat recovery. Energy Conv Manag 2013;76:234-43. doi: 10.1016/j.enconman.2013.07.036.

[28] Shu GQ, Liu LN, Tian H, Wei HQ, Xu XF. Performance comparison and working fluid analysis of subcritical and transcritical dual-loop organic Rankine cycle (DORC) used in engine waste heat recovery. Energy Conv Manag 2013;74:35-43. doi: 10.1016/j.enconman.2013.04.037.

[29] Tian H, Chang LW, Gao YY, Shu GQ, Zhao MR, Yan NH. Thermo-economic

analysis of zeotropic mixtures based on siloxanes for engine waste heat recovery using a dual-loop organic Rankine cycle (DORC). Energy Conv Manag 2017;136:11-26. doi: 10.1016/j.enconman.2016.12.066.

[30] Yang FB, Zhang HG, Yu ZB, Wang EH, Meng FX, Liu HD, Wang JF. Parametric optimization and heat transfer analysis of a dual loop ORC (organic Rankine cycle) system for CNG engine waste heat recovery. Energy 2017;118:753-75. doi: 10.1016/j.energy.2016.10.119.

[31] Song J, Gu CW. Parametric analysis of a dual loop Organic Rankine Cycle (ORC) system for engine waste heat recovery. Energy Conv Manag 2015;105:995-1005. doi: 10.1016/j.enconman.2015.08.074.

[32] Song J, Gu CW. Performance analysis of a dual-loop organic Rankine cycle (ORC) system with wet steam expansion for engine waste heat recovery. Appl Energy 2015;156:280-9. doi: 10.1016/j.apenergy.2015.07.019.

[33] Zhou YD, Wu YD, Li F, Yu LJ. Performance analysis of zeotropic mixtures for the dual-loop system combined with internal combustion engine. Energy Conv Manag 2016;118:406-14. doi:10.1016/j.enconman.2016.04.006.

[34] Ge Z, Li J, Liu Q, Duan YY, Yang Z. Thermodynamic analysis of dual-loop organic Rankine cycle using zeotropic mixtures for internal combustion engine waste heat recovery. Energy Conv Manag 2018;166:201-14. doi:10.1016/j.enconman.2018.04.027.

[35] Habibi H, Chitsaz A, Javaherdeh K, Zoghi M, Ayazpour M. Thermo-economic analysis and optimization of a solar-driven ammonia-water regenerative Rankine cycle and LNG cold energy. Energy 2018;149:147-60. doi: 10.1016/j.energy.2018.01.157.

[36] Sadreddini A, Ashjari MA, Fani M, Mohammadi A. Thermodynamic analysis of a new cascade ORC and transcritical CO2 cycle to recover energy from medium temperature heat source and liquefied natural gas. Energy Conv Manag 2018;167:9-20. doi: 10.1016/j.enconman.2018.04.093.

[37] Cao Y, Ren JQ, Sang YQ, Dai YP. Thermodynamic analysis and optimization of a gas turbine and cascade CO2 combined cycle. Energy Conv Manag 2017;144:193-204. doi: 10.1016/j.enconman.2017.04.066.

[38] Yuan Y, Xu G, Quan Y, Wu H, Song G, Gong W, Luo X. Performance analysis of

a new deep super-cooling two-stage organic Rankine cycle. Energy Conv Manag 2017;148:305-16. doi:10.1016/j.enconman.2017.06.006.

[39] Xia JX, Wang JF, Lou JW, Zhao P, Dai YP. Thermo-economic analysis and optimization of a combined cooling and power (CCP) system for engine waste heat recovery. Energy Conv Manag 2016;128:303-16. doi: 10.1016/j.enconman.2016.09.086.

[40] Wu C, Wang SS, Feng XJ, Li J. Energy, exergy and exergoeconomic analyses of a combined supercritical CO2 recompression Brayton/absorption refrigeration cycle. Energy Conv Manag 2017;148:360-77. doi: 10.1016/j.enconman.2017.05.042.

[41] NREL. System Advisor Model, http://sam.nrel.gov; [accessed 25 May 2018].

[42] NREL. System Advisor Model User Documentation, Help Contents. Version 2017.9.5.

[43] Kutscher C, Burkholder F, Stynes K. Generation of a parabolic trough collector efficiency curve from separate measurements of outdoor optical efficiency and indoor receiver heat loss. NREL/CP-5500-49304, 2010.

[44] Price H. A parabolic trough solar power plant simulation model. NREL/CP-550-33209, 2003.

[45] Burkholder F, Kutscher C. Heat loss testing of Schott’s 2008 PTR70 parabolic trough receiver. NREL/TP-550-45633, 2009.

[46] Petr V, Kolovratnik M. Wet steam energy loss and related Baumann rule in low pressure steam turbines. Proc Inst Mech Eng Part A-J Power Energy 2014;228:206-15. doi:10.1177/0957650913512314.

[47] Macchi E, Astolfi M. Organic Rankine Cycle (ORC) Power Systems, Technologies and Applications. Woodhead Publishing; 2017.

[48] Chen HJ, Goswami DY, Stefanakos EKA. A review of thermodynamic cycles and working fluids for the conversion of low-grade heat. Renew Sust Energ Rev 2010;14:3059-67. doi:10.1016/j.rser.2010.07.006.

[49] Rahbar K, Mahmoud S, Al-Dadah RK, Moazami N, Mirhadizadeh SA. Review of organic Rankine cycle for small-scale applications. Energy Conv Manag 2017;134:135-55. doi: 10.1016/j.enconman.2016.12.023.

[50] Yilmaz IH, Soylemez MS. Thermo-mathematical modeling of parabolic trough collector. Energy Conv Manag 2014;88:768-84. doi:10.1016/j.enconman.2014.09.031.

[51] Barbero R, Rovira A, Montes MJ, Val JMM. A new approach for the prediction of thermal efficiency in solar receivers. Energy Conv Manag 2016;123:498-511. doi:10.1016/j.enconman.2016.06.065.

[52] Liu QB , Yang ML, Lei J, Jin HG, Gao ZC, Wang YL. Modeling and optimizing parabolic trough solar collector systems using the least squares support vector machine method. Sol Energy 2012;86:1973-80. doi:10.1016/j.solener.2012.01.026.

[53] Shouhang Dunhuang 10 MW Phase I, https://solarpaces.nrel.gov/shouhang-dunhuang-10-mw-phase-i; 2016 [accessed November 20, 2018].

[54] Supcon Delingha 10MW Phase I, http://helioscsp.com/china-first-operational-10mw-tower-concentrated-solar-power-molten-salt-plant-in-delingha/; 2016 [accessed November 20, 2018].

[55] Popov D, Borissova A. Innovative configuration of a hybrid nuclear-solar tower power plant. Energy 2017;125:736-46. doi: 10.1016/j.energy.2017.02.147.

[56] Sun WQ, Yue XY, Wang YH. Exergy efficiency analysis of ORC (Organic Rankine Cycle) and ORC-based combined cycles driven by low-temperature waste heat. Energy Conv Manag 2017;135:63-73. doi: 10.1016/j.enconman.2016.12.042.